J|A|C|S
ARTICLES
Published on Web 04/07/2007

# Molecular Basis for Water-Promoted Supramolecular Chirality Inversion in Helical Rosette Nanotubes

Ross S. Johnson,[†,‡] Takeshi Yamazaki,[†,#] Andriy Kovalenko,[†,#] and Hicham Fenniri*[,†,‡]

*Contribution from the National Institute for Nanotechnology, Department of Chemistry, and Department of Mechanical Engineering, University of Alberta, 11421 Saskatchewan Drive, Edmonton, Alberta, T6G 2M9, Canada*

Received January 27, 2007; E-mail: hicham.fenniri@ualberta.ca

***Abstract:*** Helical rosette nanotubes (RNTs) are obtained through the self-assembly of the G∧C motif, a self-complementary DNA base analogue featuring the complementary hydrogen bonding arrays of both guanine and cytosine. The first step of this process is the formation of a 6-membered supermacrocycle (rosette) maintained by 18 hydrogen bonds, which then self-organizes into a helical stack defining a supramolecular sextuple helix whose chirality and three-dimensional organization arise from the chirality, chemical structure, and conformational organization of the G∧C motif. Because a chiral G∧C motif is predisposed to express itself asymmetrically upon self-assembly, there is a natural tendency for it to form one chiral RNT over its mirror image. Here we describe the synthesis and characterization of a chiral G∧C motif that self-assembles into helical RNTs in methanol, but undergoes mirror image supramolecular chirality inversion upon the addition of very small amounts of water (<1% v/v). Extensive physical and computational studies established that the mirror-image RNTs obtained, referred to as *chiromers*, result from thermodynamic (in water) and kinetic (in methanol) self-assembly processes involving two conformational isomers of the parent G∧C motif. Although derived from conformational states, the chiromers are thermodynamically stable supramolecular species, they display dominant/recessive behavior, they memorize and amplify their chirality in an achiral environment, they change their chirality in response to solvent and temperature, and they catalytically transfer their chirality. On the basis of these studies, a detailed mechanism for supramolecular chirality inversion triggered by specific molecular interactions between water molecules and the G∧C motif is proposed.

## Introduction

Supramolecular chirality (SC)[1] is the expression of absolute molecular chirality at the macromolecular level and generally results from the self-assembly of multiple copies of one or more chiral components or from the self-organization of chiral oligomeric systems (e.g., polymers, biopolymers). While there is literature precedent for solvent-induced chirality inversion, most of these reports dealt with host−guest complexes,[2] polymers,[3] biopolymers,[4] liquid crystalline phases,[5] or thin polymer films,[3a,g,i] and provided limited mechanistic insight as to the role of solvent at the intermolecular level. The system

[†] National Institute for Nanotechnology.
[‡] Department of Chemistry.
[#] Department of Mechanical Engineering.

(1) (a) Green, M. M.; Peterson, N. C.; Sato, T.; Teramoto, A.; Cook, R.; Lifson, S. *Science* **1995**, *268*, 1860−1866. (b) Ferringa, B. L.; van Delden, R. A. *Angew. Chem., Int. Ed.* **1999**, *38*, 3419−3438. (c) Yashima, E.; Maeda, K.; Nishimura, T. *Chem.*−*Eur. J.* **2004**, *10*, 42−51. (d) Hill, D. J.; Mio, M. J.; Prince, R. B.; Hughes, T. S.; Moore, J. S. *Chem. Rev.* **2001**, *101*, 3893−4011. (e) Borovkov, V. V.; Hembury, G. A.; Inoue, Y. *Acc. Chem. Res.* **2004**, *37*, 449−459. (f) Hof, F.; Craig, S.-L.; Nuckolls, C.; Rebek, J., Jr. *Angew. Chem., Int. Ed.* **2002**, *41*, 1488−1508. (g) Kikuchi, Y.; Kobayashi, K.; Aoyama, Y. *J. Am. Chem. Soc.* **1992**, *114*, 1351−1358. (h) Yashima, E.; Maeda, K.; Okamato, Y. *Nature* **1999**, *399*, 449−451. (i) Prins, L. J.; De Jong, F.; Timmerman, P.; Reinhoudt, D. N. *Nature* **2000**, *408*, 181−184. (j) Lauceri, R.; Raudino, A.; Scolaro, L. M.; Micali, N.; Purello, R. *J. Am. Chem. Soc.* **2002**, *124*, 894−895. (k) Huck, N. P. M.; Jager, W. F.; de Lange, B.; Feringa, B. L. *Science* **1996**, *273*, 1686−1688. (l) Ribó, J. M.; Crusats, J.; Sagués, F.; Claret, J.; Rubires, R. *Science* **2001**, *292*, 2063−2066. (m) Zahn, S.; Canary, J. W. *Science* **2000**, *288*, 1404−1407. (n) de Jong, J. J. D.; Lucas, N. L.; Kellogg, R. M.; van Esch, J. H.; Feringa, B. L. *Science* **2004**, *304*, 278−281. (o) Goto, H.; Yashima, E. *J. Am. Chem. Soc.* **2002**, *124*, 7943−7949. (p) Holmes, A. E.; Barcena, H.; Canary, J. W. *Adv. Supramol. Chem.* **2002**, *8*, 43−78. (q) Sakurai, S.; Okoshi, K.; Kumaki, J.; Yashima, E. *J. Am. Chem. Soc.* **2006**, *128*, 5650−5651.

(2) (a) Borovkov, V. V.; Hembury, G. A.; Inoue, Y. *Angew. Chem., Int. Ed.* **2003**, *115*, 5468−5472. (b) Boiadjiecv, S. E.; Lightner, D. A. *J. Am. Chem. Soc.* **2000**, *122*, 378−383.

(3) (a) Satrijo, A.; Meskers, S. C. J.; Swager, T. M. *J. Am. Chem. Soc.* **2006**, *128*, 9030−9031. (b) Goto, H.; Okamoto, Y.; Yashima, E. *Macromolecules* **2002**, *35*, 4590−4601. (c) Langeveld-Voss, B. M. W.; Christiaans, M. P. T.; Janssen, R. A. J.; Meijer, E. W. *Macromolecules* **1998**, *31*, 6702−6704. (d) Price, C. C.; Osgan, M. *J. Am. Chem. Soc.* **1956**, *78*, 4789−4790. (e) Furukawa, J. In *Optically Active Polymers*; Sélégny, E., Ed.; D. Reidel Publishing Co.: Dordrecht, The Netherlands, 1979; pp 317−330. (f) Pu, L. *Acta Polym.* **1997**, *8*, 116−141. (g) Bouman, M. M.; Meijer, E. W. *Adv. Mater.* **1995**, *7*, 385−387. (h) Bidan, G.; Guillerez, S.; Sorokin, V. *Adv. Mater.* **1996**, *8*, 157−160. (i) Kajitani, T.; Okoshi, K.; Sakurai, S.; Kumaki, J.; Yashima, E. *J. Am. Chem. Soc.* **2006**, *128*, 708−709. (j) Sakurai, S.; Okoshi, K.; Kumaki, J.; Yashima, E. *J. Am. Chem. Soc.* **2006**, *128*, 5650−5651. (k) Lam, J. W. Y.; Tang, B. Z. *Acc. Chem. Res.* **2005**, *38*, 745−754. (l) Fujiki, M.; Koe, J. R.; Motonaga, M.; Nakashima, H.; Terao, K.; Teramoto, A. *J. Am. Chem. Soc.* **2001**, *123*, 6253−6261. (m) Nakako, H.; Nomura, R.; Masuda, T. *Macromolecules* **2001**, *34*, 1496−1502. (n) Cheuk, K. K. L.; Lam, J. W. Y.; Chen, J.; Lai, L. M.; Tang, B. Z. *Macromolecules* **2003**, *36*, 9752−9762. (o) Maeda, K.; Mochizuki, H.; Watanabe, M.; Yashima, E. *J. Am. Chem. Soc.* **2006**, *128*, 7639−7650. (p) Okoshi, K.; Sakurai, S.; Ohsawa, S.; Kuwaki, J.; Yashima, E. *Angew. Chem., Int. Ed.* **2006**, *45*, 1−5. (q) Nakashima, H.; Fujiki, M.; Koe, J. R.; Motonaga, M. *J. Am. Chem. Soc.* **2001**, *123*, 1963−1969.

***Scheme 1.*** Line Structures of Compounds **1**−**3** and Synthesis of Compound **3**[a]

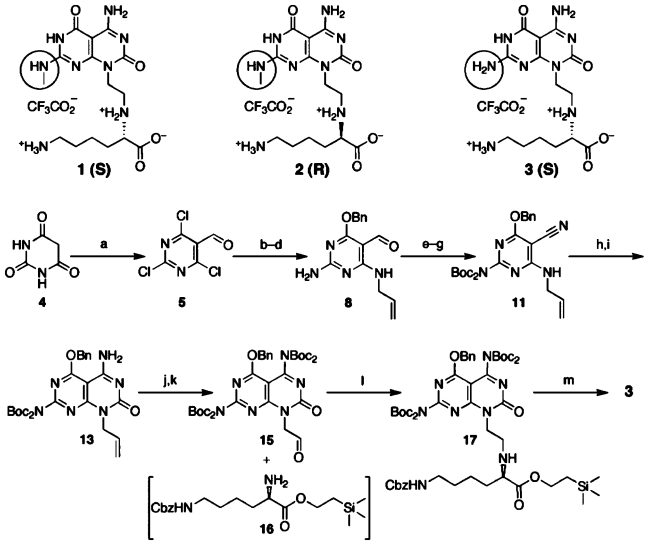


[a] Conditions: (a) **4**, $POCl_3$, DMF, 70%; (b) **5**, allylamine, DCM, −78 °C, 79%; (c) **6**, $NH_4OH$, EtOH, 0 °C, 65%; (d) **7**, BnOH, NaH, THF, reflux, 76%; (e) **8**, $Boc_2O$, DMAP, $Et_3N$, THF, room temp, 72%; (f) **9**, $NH_2OH$-HCl, pyridine, room temp; (g) **10**, TFFA, THF, reflux, 89% (two steps); (h) **11**, *N*-chlorocarbonyl isocyanate, DCM, 0 °C, 62%; (i) **12**, $NH_3$/MeOH (7 M), room temp, 77%; (j) **13**, $Boc_2O$, DMAP, $Et_3N$, THF, room temp, 74%; (k) **14**, $OsO_4$, NMMO, THF/*t*−BuOH then $NaIO_4$, DCM/$H_2O$, room temp, 54%; (l) **15**, **16**, $NaBOAc_3H$, DIEA, 1,2-DCE, room temp, 65%; (m) **17**, thioanisole/TFA (6%), room temp, 78% (based on **3**·3.5TFA·1.5$H_2O$).

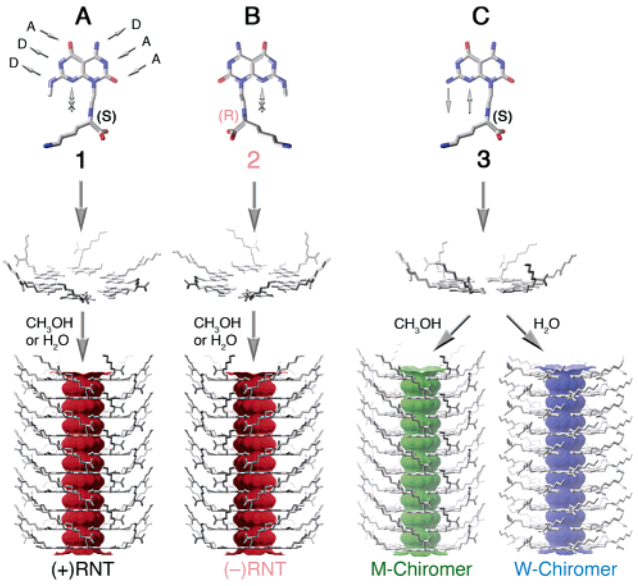


***Figure 1.*** Self-assembly of G∧C base derivatives **1**−**3** in water and methanol. Letters D and A denote donor/acceptor of H-bonds. Compounds **1** and **2** self-assemble into mirror image helical rosette nanotubes (RNTs) in both water and methanol, with no change in the CD profile. The SC inversion observed with **3** could result from its self-assembly into left- or right-handed helical RNTs, to which we refer here as W-chiromer (in water) and M-chiromer (in methanol).[10] Note that the only difference between **1** and **3** is the exocyclic $NHCH_3$ group. Because of this structural difference, **3** could in principle engage in two additional H-bonds (silver arrows), whereas **1** and **2** cannot for steric reasons.

described here deals with the hierarchical self−assembly of a small molecule whose SC crosses the mirror plane upon specific interaction with water molecules. These studies led us to propose novel mechanisms for SC inversion and catalytic transfer.

## Results

**Synthesis.** Compounds **1**, **2**, and **5**[6−8]were prepared according to previously reported procedures. Compound **3** was prepared in 13 steps and 72% average stepwise yield (Scheme 1). First, barbituric acid was converted in 70% yield to 2,4,6-trichloropyrimidine-5-carbaldehyde (**5**). Three consecutive nucleophilic aromatic substitutions on this compound afforded compound **8** in 39% yield (three steps). Selective protection of the primary amine followed by oxime synthesis and dehydration yielded **11** in 64% (three steps). Reaction with *N*-chlorocarbonyl isocyanate under basic conditions followed by cyclization in a concentrated methanolic solution of ammonia yielded a key intermediate in the preparation of G∧C base derivatives, 1,2-dihydropyrimido-[4,5-*d*]pyrimidine (**13**) in 48% yield (two steps). Boc protection of the free amino group followed by Lemieux−Johnson conversion of the allyl group to the corresponding aldehyde gave **15** in 40% yield (two steps). Reductive amination with the partially protected lysine **16** followed by deprotection in 5% thioanisole/trifluroacetic acid yielded the final product **3** in 51% (two steps).

**Solvent-Induced SC Inversion.** G∧C derivatives **1** and **2** (Figure 1) undergo hierarchical self-assembly to form a six-membered supermacrocycle maintained by 18 H-bonds,[6−9] which then self-organizes into remarkably stable,[6,7] autocatalytic,[8] helical rosette nanotubes (RNTs) in water and methanol.[6−8] In agreement with basic SC principles,[1,6−8] compound **1** and its mirror image D-isomer **2** self-assemble into nanotubular architectures with opposite helicities in water or methanol (Figure 1A,B). While compounds **1** and **2** featured CD spectra whose sign and profile were not altered in both water and methanol (Figure 2A,B), compound **3** underwent mirror image CD inversion upon switching the solvent from methanol to water

(4) (a) Pohl, F. M.; Jovin, T. M. *J. Mol. Biol.* **1972**, *67*, 375−396. (b) Cosstick, R.; Eckstein, F. *Biochemistry* **1985**, *24*, 3630−3638. (c) Okamoto, Y.; Nakano, T.; Ono, E.; Hatada, K. *Chem. Lett.* **1991**, 525−528. (d) Steinberg, I. Z.; Harrington, W. F.; Berger, A.; Sela, M.; Katchalski, E. *J. Am. Chem. Soc.* **1960**, *82*, 5263−5279. (e) Blout, E. R.; Carver, J. P.; Gross, J. *J. Am. Chem. Soc.* **1963**, *85*, 644−646. (f) Gratzer, W. B.; Rhodes, W.; Fasman, G. D. *Biopolymers* **1963**, *1*, 319−330. (g) Letsinger, R. L. *Proc. Robert A. Welch Found. Conf. Chem. Res.* **1985**, *29*, 459. (h) McIntosh, L. P.; Zielinski, W. S.; Kalish, B. W.; Pfiefer, G. P.; Sprinzl, M.; van de Sande, J. H.; Jovin, T. M. *Biochemistry* **1985**, *24*, 4806−4814. (i) Pu, Y.-M.; McDonagh, A. F.; Lightner, D. A. *J. Am. Chem. Soc.* **1993**, *115*, 377−380.
(5) (a) Celebre, G.; De Luca, G.; Maiorino, M.; Iemma, F.; Ferrarini, A.; Pieraccini, S.; Spada, G. P. *J. Am. Chem. Soc.* **2005**, *127*, 11736−11744. (b) Slaney, A. J.; Nishiyama, I.; Styring, P.; Goodby, J. W. *J. Mater. Chem.* **1992**, *2*, 805−810. (c) Loubser, C.; Wessels, P. L.; Styring, P.; Goodby, J. W. *J. Mater. Chem.* **1994**, *4*, 71−79. (d) Radley, K.; McLay, N. *J. Phys. Chem.* **1994**, *98*, 3071−3072.
(6) (a) Fenniri, H.; Deng, B. L.; Ribbe, A. E.; Hallenga, K.; Jacob, J.; Thiyagarajan, P. *Proc. Natl. Acad. Sci. U.S.A.* **2002**, *99* (suppl. 2), 6487−6492. (b) Fenniri, H.; Mathivanan, P.; Vidale, K. L.; Sherman, D. M.; Hallenga, K.; Wood, K. V.; Stowell, J. G. *J. Am. Chem. Soc.* **2001**, *123*, 3854−3855.
(7) Moralez, J. G.; Raez, J.; Yamazaki, T.; Motkuri, R. K.; Kovalenko, A.; Fenniri, H. *J. Am. Chem. Soc.* **2005**, *127*, 8307−8309.
(8) Fenniri, H.; Deng, B. L.; Ribbe, A. E. *J. Am. Chem. Soc.* **2002**, *124*, 11064−11072.
(9) (a) Lawrence, D. S.; Jiang, T.; Levett, M. *Chem. Rev.* **1995**, *95*, 2229−2260. (b) Ducharme, Y.; Wuest, J. D. *J. Org. Chem.* **1988**, *53*, 5787−5789. (c) Zerkowski, J. A.; Seto, C. T.; Whitesides, G. M. *J. Am. Chem. Soc.* **1992**, *114*, 5473−5475. (d) Zimmerman, S. C.; Duerr, B. F. *J. Org. Chem.* **1992**, *57*, 2215−2217. (e) Bonazzi, S.; De Morais, M. M.; Gottarelli, G.; Mariani, P.; Spada, G. P. *Angew. Chem., Int. Ed.* **1993**, *32*, 248−250. (f) Yang, J.; Marendaz, J.−L.; Geib, S.−J.; Hamilton, A. D. *Tetrahedron Lett.* **1994**, *35*, 3665−3668. (g) Prins, L. J.; Timmerman, P.; Reinhoudt, D. N. *Pure Appl. Chem.* **1998**, *70*, 1459−1468. (h) Davis, J. T. *Angew. Chem., Int. Ed.* **2006**, *43*, 668−698. (i) Marsh, A.; Silvestri, M.; Lehn, J.−M. *Chem. Commun.* **1996**, 1527−1528. (j) Mascal, M.; Hext, N. M.; Warmuth, R.; Moore, M. H.; Turkenburg, J. P. *Angew. Chem., Int. Ed.* **1996**, *35*, 2204−2206.

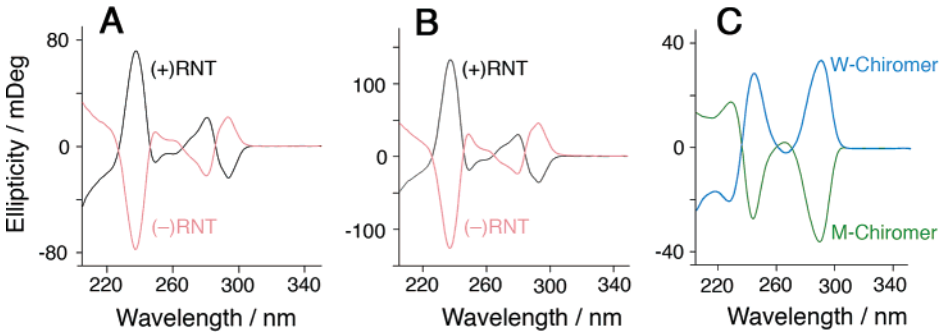


***Figure 2.*** CD spectra of **1**−**3** in water and methanol. The CD spectra of **1** ($6.8 \times 10^{-5}$ M, black) and **2** ($6.8 \times 10^{-5}$ M, pink) in water (A) and MeOH (B) grew over time reaching their maximum intensity over a period of 1 month at 20 °C. The higher ellipticity in methanol reflects the formation of much longer RNTs in this solvent. The CD spectra of **3** ($4.0 \times 10^{-5}$ M) in water (blue, W-chiromer) and methanol (green, M-chiromer) were recorded after aging the water stock solution ($1.3 \times 10^{-3}$ M, 1 mg/mL) for 840 h and the methanol stock solution ($1.3 \times 10^{-3}$ M, 1 mg/mL) for 5 h, at 20 °C (C).

(and vice versa). Although unexpected, this observation was critical in developing a molecular model and a mechanism for this solvent-induced SC inversion (vide infra). The methanol chiromer[10] (M-chiromer) in Figure 2C shows two minima (−39.4 mdeg at 289 nm, −31.1 mdeg at 244 nm), and one maximum (19.6 mdeg at 229 nm), whereas the water chiromer (W-chiromer) gave a mirror image profile (37.7 mdeg at 290 nm, 32.0 mdeg at 244 nm, −22.8 mdeg at 228 nm).

Time-dependent CD experiments established that this is not a random process (Supporting Information Figure S1), and variable temperature CD experiments (Figure S2) established that the observed chirality is supramolecular in nature as it disappears upon heating and is restored upon cooling. Since the absolute chirality of **3** cannot reversibly invert upon switching solvents, it was logical to postulate that the conformation of **3** within the supramolecular architecture is such that circularly polarized light interacts with chromophores in mirror image spaces in water and methanol, respectively, regardless of the absolute molecular chirality of **3**.

**The Chiromers Display the Same Hierarchical Organization.** The hypothesis of a conformationally-driven chirality inversion implies that the chiromers maintain the same hierarchical organization and that **3** self-assembles into a rosette supermacrocycle, which in turn self-organizes into pseudomirror image tubular stacks in water and methanol. As a result, we anticipated the chiromers to display similar NMR spectra and physical dimensions. NOESY NMR experiments established that compound **3** does indeed form key H-bonds[6,7] characteristic of the rosette assembly in 90% $H_2O/D_2O$ and in $CD_3OH$ (Figure 3).

As shown in Figure 4 (and Figure S3−S11) tapping mode AFM, TEM, and SEM imaging of **3** established the formation of RNTs with identical outer diameters in water and methanol: 3.6 nm by AFM and 3.8 nm by TEM, in agreement with the calculated van der Waals diameter of 3.7 nm. UV−vis spectra of **3** in water and methanol featured essentially the same profiles. A hypochromic effect (20%) and a small red shift (7 nm) were noted in methanol, indicating advanced aggregation in this solvent (Figure S12).[6] These results confirm that the supramolecular architectures in water and methanol have the same hierarchical organization, dimensions, and shape. Therefore, the observed chirality inversion is associated with stable, solvent-dependent conformational states, to which we refer here as W-chiromer (in water) and M-chiromer (in methanol).[10] To better define these states, the effect of solvation free energy was investigated first to identify the dominant/recessive chiromer. Second, the ability of the chiromers to memorize[1h] their SC was established. Third, the effect of temperature was investigated to establish the kinetic/thermodynamic pathways leading to the chiromers. Finally, the ability of the thermodynamic (dominant) chiromer to catalytically transfer its chirality to the kinetic (recessive) one was demonstrated.

**Water Leads to the Formation of the Dominant Chiromer.** This experiment consisted in preparing nine samples of **3** (1 mg/mL, $1.3 \times 10^{-3}$ M) varying in water (methanol) content from 100% (0%) to 0% (100%) and monitoring their CD spectra over time. After 24 h (and over a period of 672 h), it was clear that water, even at 1% of the total volume, was the dominant solvent (Figures 5A, S13). The opposite SC appeared when methanol exceeded 99% (v/v). Particularly noteworthy, is the accelerating effect of methanol on the formation of the RNTs as can be inferred from the faster growth of the CD profile between 0−95% methanol (Figures S13, S14). Time-dependent dynamic light scattering (Figure 5B) and SEM studies (Figures S6−S11) established that the accelerating effect of methanol is associated with the formation of longer RNTs. In summary this study (a) has shown that very small amounts of water (1% v/v) induced SC inversion of the M-chiromer thereby suggesting a specific role for this solvent and confirmed (b) that chiromerism is not a random process and (c) that there are two chiromers with opposite chiroptical properties, whose formation is controlled by their solvation free energy, as well as by the kinetics/thermodynamics of RNT self-assembly. These results also suggest that the formation of the M-chiromer is under kinetic control.

**Chiromerism Results from Conformational Memory.** This experiment was designed to test the ability of the chiromers to memorize their SC in a solvent that induces the opposite chirality. Thus, compound **3** ($1.3 \times 10^{-3}$ M, 1 mg/mL) was dissolved in methanol and water and allowed to equilibrate (672 h) before an aliquot (62.5 $\mu$L) from each solution was transferred to the solvent that induces opposite SC (1937.5 $\mu$L, 97% final volume). The SC of the water/methanol (3:97) sample of **3** ($4.0 \times 10^{-5}$ M) decreased initially over 168 h, then increased significantly, well beyond the initial value (Figure S16), thus

(10) The term chiromerism was introduced to express the notions of chirality and chimerism. That is the ability of a single chiral molecule to express multiple, yet thermodynamically stable, supramolecular chirality outputs as a result of preferred conformational states under a set of physical conditions. Chiromers are supramolecular conformational isomers that (a) are thermodynamically stable, (b) can memorize their chirality, and (c) can amplify their chirality in an achiral environment.

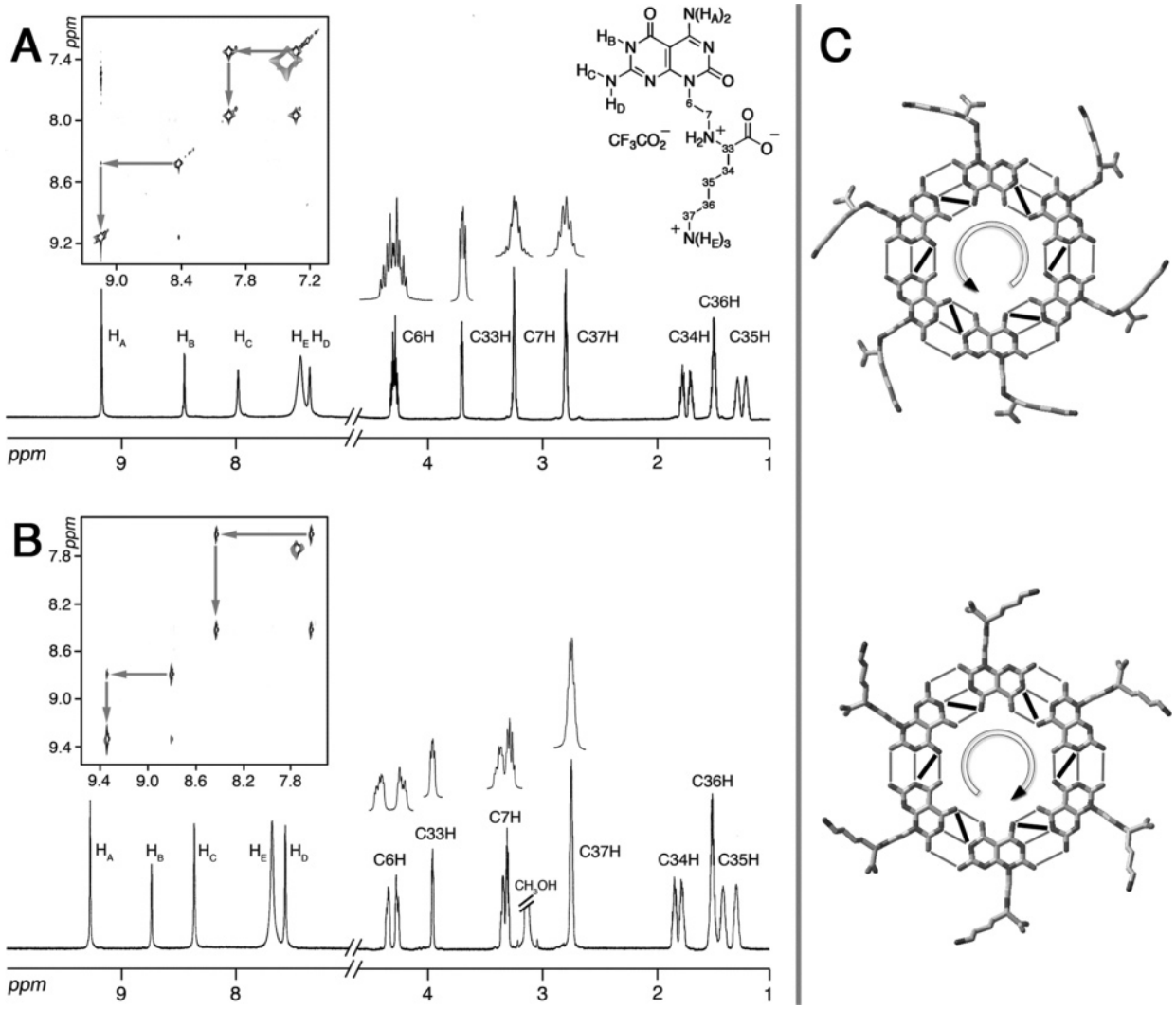


***Figure 3.*** One-dimensional $^1$H NMR and section of the NOESY spectrum in 90% $H_2O/D_2O$ (A) and in $CD_3OH$ (B) showing evidence of the formation of the proposed H-bond network (C). The NOESY spectra show NOEs between $H_A$ and $H_B$ (dark bars in C). Since these protons are too far apart to display any intramodular NOEs, the observation of an NOE between them confirms the existence of intermodular H-bonds. In addition, no other NOEs or imino proton signals resulting from nonassembled **3** or nonspecific aggregates thereof were observed. These results are diagnostic of the formation of the rosette assembly.[6,7]

confirming the ability of the W-chiromer to memorize its SC. The initial decrease in SC is possibly the result of a small amount of nonassembled **3** in the parent water stock solution, which upon dilution in methanol, undergoes self-assembly into the M-chiromer, thus attenuating the system's overall SC. Subsequent growth of the CD profile beyond the initial phase confirms the accelerating effect of methanol on RNT growth and suggests a catalytic interconversion of chiromers (vide infra).

While the M-chiromer ($4.0 \times 10^{-5}$ M) maintained its SC in methanol/water (3:97), the intensity of the CD profile decreased steadily over the course of the experiment (Figure S16), eventually disappearing after 8 weeks with no restoration or inversion even after 7 months. The fact that the CD profile of the M-chiromer disappears over time suggests an equilibrium for chiromer interconversion involving unassembled **3** as an intermediate species, since the latter does not self-assemble at CD concentration. However, when 90% of the solvent was evaporated, the residue aged for 2 weeks, then rediluted in water ($4.0 \times 10^{-5}$ M), its CD profile was not only restored, but was indeed that of the W-chiromer. These experiments confirm that (a) W-chiromer is the thermodynamic product whereas the M-chiromer is the kinetic product, (b) W-chiromer is kinetically and thermodynamically stable, (c) water is the dominant solvent, (d) methanol accelerates RNT growth, and (e) chiromerism is the result of two distinct, "mirror image", stable, and solvent-dependent conformational states.

**Kinetic versus Thermodynamic Control of Hierarchical Self-Assembly.** Solutions of **3** ($1.3 \times 10^{-3}$ M, 1 mg/mL) in methanol and in water were each split into two equal-volume samples, the first was kept at 20 °C while the other was refluxed for 3 s. Aliquots (62.5 $\mu$L) from the water and methanol solutions were diluted in the same solvents (1937.5 $\mu$L, $[3]_{final} = 4.0 \times 10^{-5}$ M) after 24, 120, 168, and 336 h and their CD spectra were recorded. The heated water samples showed a large increase (300−400%) in the CD intensity and no change in profile over a period of 336 h (Figure S16). Conversely, the heated methanol samples adopted the opposite SC (Figure 5C). This thermally-induced chirality inversion was found to take place only for stock solutions aged for less than 72 h. Samples aged for more than 72 h became stereochemically locked (Figure S18). Regardless of the age and thermal treatment, SEM imaging

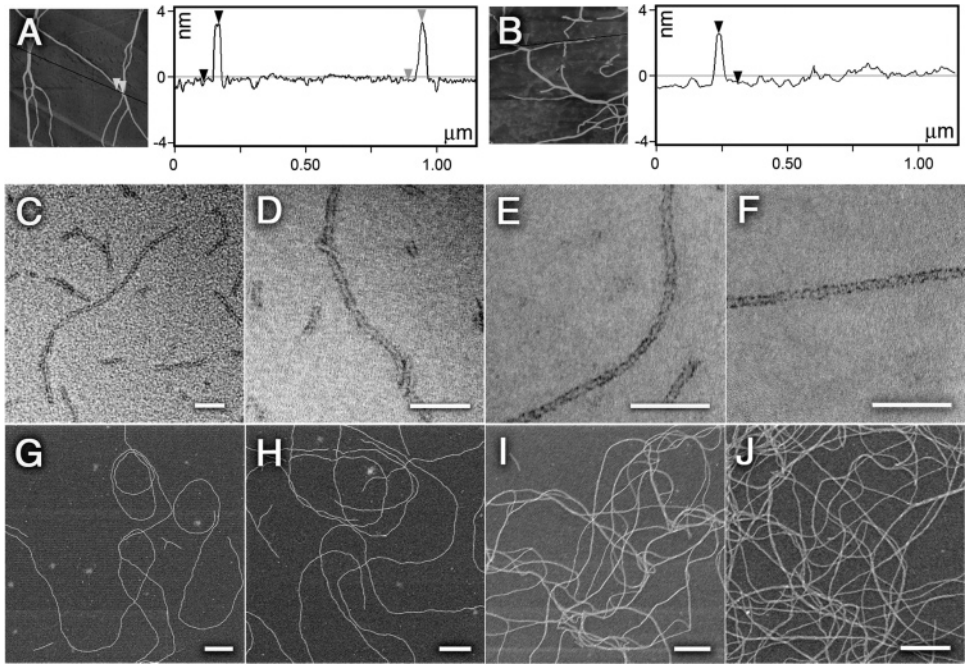


***Figure 4.*** TM-AFM (A, B), TEM (C-F), and SEM (G-J) images of W-chiromer (A, C, D, G, H) and M-chiromer (B, E, F, I, J) establishing their identical dimensions and hierarchical organization. TM-AFM images show that the chiromers have very similar outer diameter, 3.58 for W-chiromer (A) versus 3.63 for M-chiromer (B). The TEM images of the W-chiromer (C, D) and M-chiromer (E, F) stained with nano-W gave the same outer diameter for both chiromers (3.8 nm). SEM images of the W-chiromer (G, H) and M-chiromer (I, J) show the formation of long nanotubes after aging for 1 month at $1.3 \times 10^{-3}$ M (1 mg/mL) and then diluting to $0.33 \times 10^{-3}$ M (0.25 mg/mL). Scale bars are 40 nm for C−F and 250 nm for G−J.

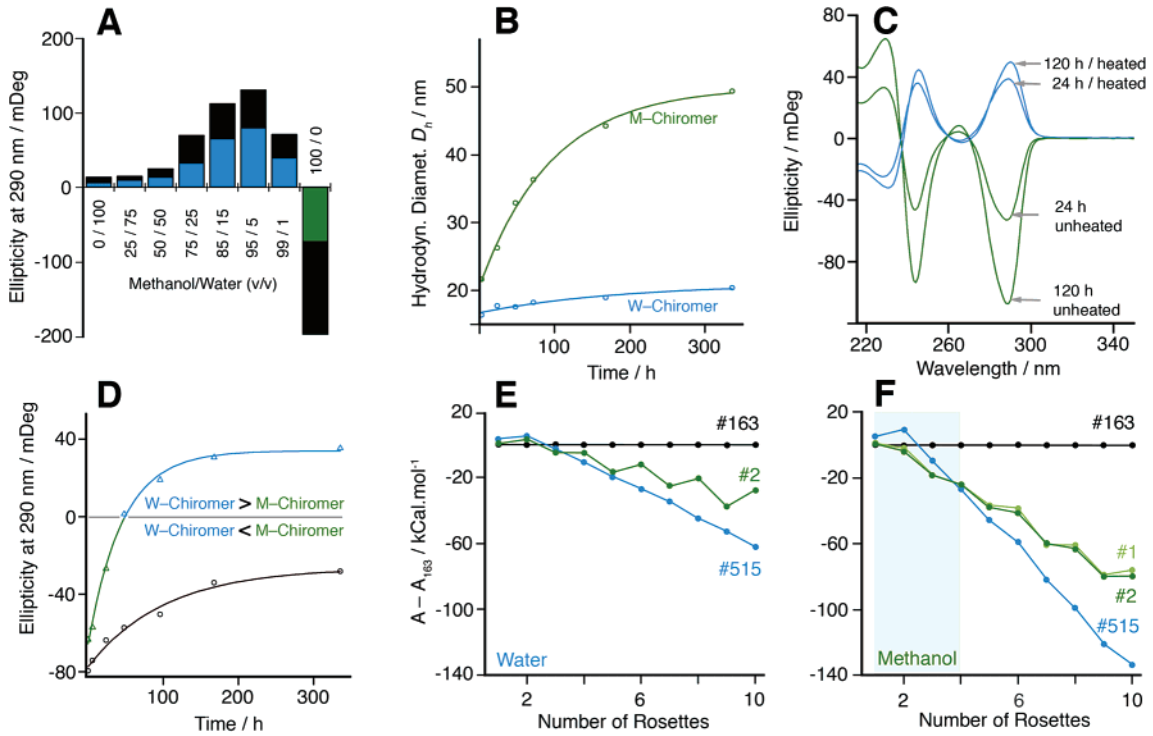


***Figure 5.*** Experiments establishing the kinetic and thermodynamic pathways leading to the M- and W-chiromers. (A) Binary solvent study showing that the W-chiromer of **3** is the dominant supramolecular isomer. The blue/green bars show the growth after 24 h at 290 nm and the black extensions show the additional growth recorded after 672 h. (B) Time-dependent hydrodynamic diameter of the W-chiromer (blue trace) and M-chiromer (green trace) monitored by DLS. (C) Thermally-induced SC inversion of the M-chiromer. The CD profiles of the heated (red traces) and nonheated (black traces) were monitored after 24 and 120 h. (D) SC inversion of M-chiromer catalyzed by W-chiromer (green/blue traces). The W-chiromer was replaced with water in the control experiment (black trace). Free energy trajectories of RNTs #1, #2, #163, and #515 relative to the most stable RNT at $N = 1$ (#163) in water (E) and methanol (F). Although RNT #515 is more stable than RNT #2 for $N > 4$, it does not form in methanol because it must overcome a significant energy barrier (gray box) during the early stages of self-assembly.

showed the formation of RNTs in all samples (Figure S11), although significantly longer in the heated samples, in agreement with DLS data (Figure S15). These studies confirmed that (a) W-chiromer and M-chiromer are one species that exists in two mirror-image, interconvertible, conformational states, (b) M-chiromer is the kinetic product and W-chiromer is the thermo-

***Scheme 2.*** Catalytic and Thermodynamic Pathways for Chiromer Formation and Interconversion in Methanol (Left) and Water (Right)[a]

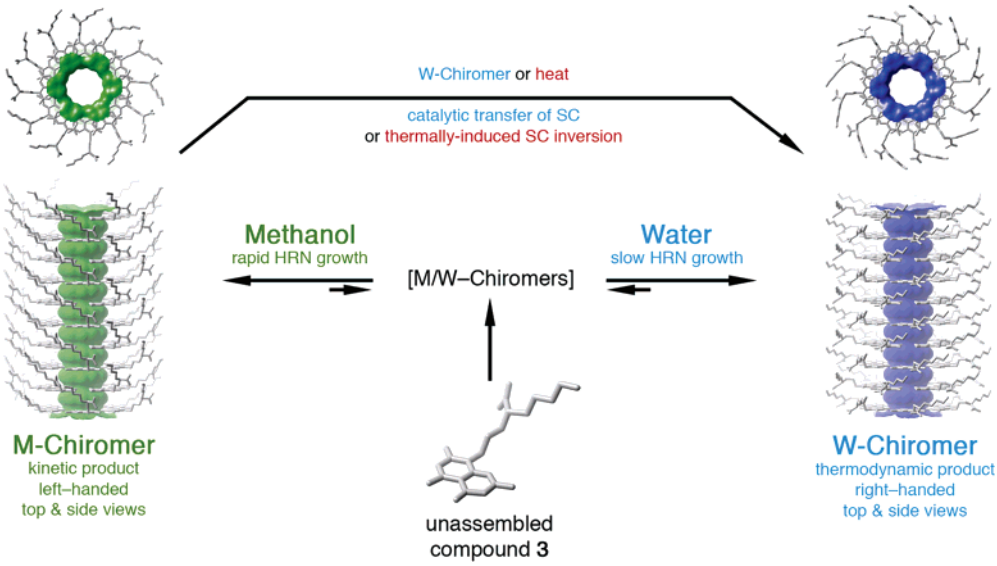


[a] Upon dissolution of compound **3** in water or methanol, both chiromers can form during the early stages of self-assembly. However, depending on the solvent and thermodynamic conditions used, only one chiromer will grow preferentially.

dynamic product, and (c) M-chiromer can cross the mirror plane before becoming kinetically and conformationally locked.

**Catalytic Transfer of Conformational Chirality.** Since the W-chiromer memorizes its SC, grows faster in the presence of methanol, and is the thermodynamic product, we tested its ability to catalyze the SC inversion of the M-chiromer. Thus, catalytic amounts of W-chiromer (10 mol %) were added to the M-chiromer and the reaction was monitored by CD. As shown in Figure 5D (and Figure S19), the M-chiromer underwent complete inversion of chirality, whereas the control experiment (without W-chiromer) underwent, as expected, an attenuation of the CD profile.

**The Chiromers Are Solvent-Stabilized Supramolecular Conformational Isomers.** Based on our experimental results, it is clear that the chiromers self-assemble into pseudomirror image RNTs. It is also clear that the water and methanol chiromers correspond to the thermodynamic and kinetic products, respectively. To uncover the structural basis for these results we carried out a conformational search in water and methanol, with the solvation structure and thermodynamics obtained by the three dimensional molecular theory of solvation (section M, Supporting Information).[7,11] The first step consisted in carrying out a conformational search around compound **3**. This motif was minimized, then 648 conformations were generated by varying dihedral angles around six bonds as shown in Figure S21. The second step consisted in arranging each of these conformations to form 6-fold symmetry rosettes maintained by 18 H-bonds. The rosettes were then stacked in a tubular fashion with an interplanar separation of 4.5 Å and a rotation angle of 30° per rosette along the main axis.[6−8] Because of severe steric constraints, only 153 of the 648 conformers could be assembled into RNTs. The third step consisted in minimizing the energy of the 153 RNTs using Macromodel 8.5/Maestro 6.0 with OPLS-AA force field.[12] The PRCG energy minimization in implicit GB/SA water was then applied to the 153 RNTs consisting each of 11 rosettes, with the top and bottom 2 rosettes as well as all the G∧C bases fixed to reduce end effects. The central rosette in each of the 153 RNTs was taken to finally construct RNTs composed of $N = 1-10$ rosettes. Finally, to obtain a detailed microscopic insight into the organization of solvent molecules around the RNTs and their role in nanotube formation, we applied the 3D-RISM−KH theory[7,11] to the 153 RNTs composed of $N$ rosettes ($N = 1-10$) in water or methanol and in the presence of $Cl^-$ counterions. The free energy of a given RNT conformer was obtained as a sum of the internal energy and the solvation free energy. Figures S22−S29 present the free energy trajectories, relative to the most stable RNT at $N = 1$ (RNT #163).

From these calculations two families of RNTs were identified, typified by (a) right-handed RNT #515, as a global thermodynamic minimum corresponding to the W-chiromer, and (b) left-handed RNT #2, as a kinetic product corresponding to the M-chiromer (Figures 1 and S30). To further substantiate this hypothesis, we have also carried out electronic structure calculations to obtain theoretical CD spectra for helically arranged motifs derived from stable RNT #515 (W-chiromer) and #2 (M-chiromer) as shown in Figures S31 and S32. The system described here is the first in which mirror-image supramolecular chirality outputs were unambiguously connected to a kinetic *versus* thermodynamic control of hierarchical self-assembly. Such control results from the self-assembly of preferred conformational states of a single homochiral molecule.

## Discussion

**A Mechanism for Chiromer Formation and Catalytic Interconversion.** On the basis of the above experimental results and computational studies, the following mechanism for chiromer formation, growth, and interconversion may be envisioned (Scheme 2, Figure 6). Dissolution of compound **3** in water leads most likely to the formation of a large population of chiromers, typified by left- and right-handed short RNTs. However, because RNT growth is significantly slower in water, and because the initial energy barriers to formation of left- and right-handed

(11) Kovalenko, A. In *Molecular Theory of Solvation*; Hirata, F., Ed.; Kluwer Academic Publishers: Dordrecht, The Netherlands, 2003; pp 169−275.
(12) Jorgensen, W. L.; Maxwell, D. S.; Tirado−Rives, J. J. *J. Am. Chem. Soc.* **1996**, *118*, 11225−11235.

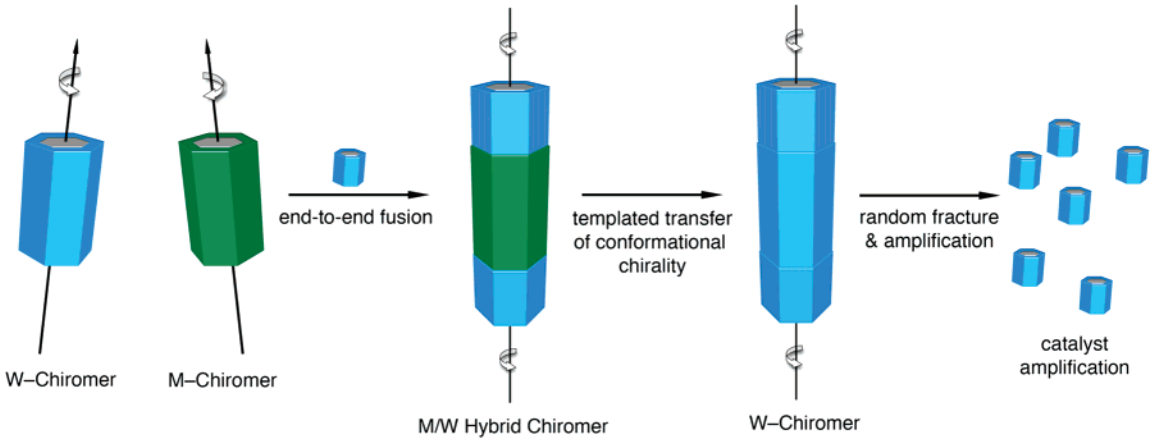


***Figure 6.*** Proposed templated supramolecular chain reaction mechanism for the catalytic transfer of conformational chirality from W-chiromer to M-chiromer.

***Table 1.*** Free Energy (kCal/mol) of Binding of Water Molecules in Unique Arrangements ($W_1$−$W_3$) and Methanol Molecules in Unique Arrangements ($M_1$, $M_2$) in the First Solvation Shell around a Single Motif in W-Chiromer (RNT #515) and M-Chiromer (RNT #2) in Water, Water−Methanol (50/50), and in Methanol

| | $H_2O$ | | $H_2O$/MeOH (50/50) | | MeOH | |
|---|---|---|---|---|---|---|
| Chiromer | W | M | W | M | W | M |
| $W_1$ | −5.03 | −5.47 | −5.51 | −6.60 | | |
| $W_2$ | −6.01 | −5.62 | −6.34 | −6.22 | | |
| $W_3$ | −5.36 | −4.59 | −6.25 | −4.72 | | |
| $\Sigma W_n$ | −16.4 | −15.7 | −18.1 | −17.5 | | |
| $M_1$ | | | −4.46 | −5.60 | −5.45 | −7.53 |
| $M_2$ | | | −5.74 | −4.29 | −7.73 | −5.37 |
| $\Sigma M_n$ | | | −10.2 | −9.9 | −13.2 | −12.9 |

RNTs are similar (Figure 5E), right-handed RNTs will form preferentially because their free energy trajectory is steeper, leading as a result to the W-chiromer (right-handed, thermodynamic product). Dissolution of **3** in methanol should also lead to the formation of both left- and right-handed short RNTs. However, because there is no energy barrier to the formation of left-handed RNTs in methanol (Figure 5F), and because methanol accelerates RNT self-assembly regardless of handedness, the left-handed population of RNTs will grow faster (kinetic pathway) and take over the SC of the system, leading as a result to the M-chiromer (left handed, kinetic product). It is also important to point out that the right-handed W-chiromer can be induced to form and grow faster in methanol if heat is applied to the solution to overcome the initial energy barrier. This heat-induced SC inversion is indeed possible if the sample is heated within 72 h of preparation. Beyond 72 h, conversion of M-chiromer into W-chiromer does not take place because (a) all traces of W-chiromer that could act as a catalyst for interconversion were converted to long and kinetically stable M-chiromer, and (b) inverting the chirality of mature M-chiromer would require overcoming its very large solvation free energy.

A simple mechanistic pathway for the conversion of M-chiromer into W-chiromer could be targeted equilibrium shifting toward the thermodynamic product, a supramolecular variation on Le Châtelier's principle (Table S2). Alternatively, an active role for the W-chiromer may also be envisioned, possibly involving: (a) the formation of a hybrid M/W-chiromer through end-to-end fusion followed by (b) cooperative transfer of conformational information from the W-chiromer to the M-chiromer via a templated supramolecular chain reaction[8] mechanism (Figure 6). The latter mechanism is more likely since (a) the formation of the M-chiromer proceeds much faster (Figure 5B), and (b) the M-chiromer used in this experiment was aged beyond the stage for interconversion (i.e., conformationally locked, Figures S18, S19).

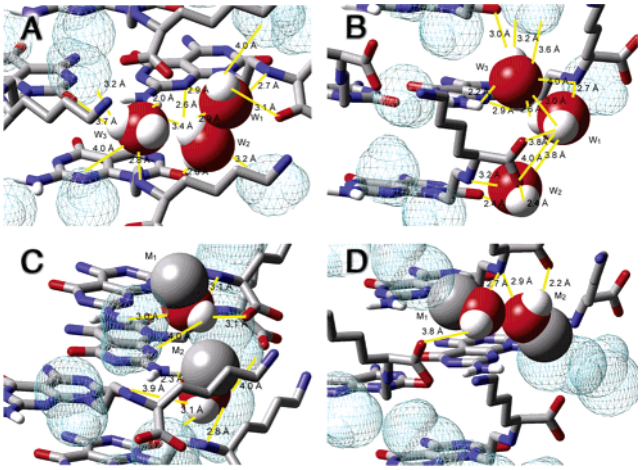


***Figure 7.*** Hydrogen-bond network generated in the first solvation shell with W-chiromer (A, C) and M-chiromer (B, D) in water (A, B) and in methanol (C, D).

**Achiral Solvent Molecules Play the Role of a Supramolecular Chirality Switch.** One important point we had to address, however, is the profound effect of an apparently small structural difference between compound **1** and **3** (a methyl group) on the RNTs' chiroptical and physical properties. The absence of the methyl group in **3** not only eliminates a hydrophobic patch, but also opens access to the pyrimidinic nitrogens thus creating two new H-bond donor/acceptor sites (see Figure 1). This triple effect should allow for a deeper penetration of solvent molecules into the walls of the RNTs where they could establish strong H-bonds. This hypothesis was probed computationally and solvation models were obtained (section N, Supporting Information). The solvation models resulted in three unique arrangements of water molecules ($W_1$−$W_3$) and two for methanol ($M_1$, $M_2$) around the chiromers (Table 1, Figure S41). As expected, most of these solvent molecules are within H-bond distances from the exocyclic amino group and/or the pyrimidinic nitrogen (Figure 7).

The proposed mechanism for chiromer formation rests on the hypothesis that W- and M-chiromers coexist in solution during the early stages of the self-assembly process and that one grows

preferentially depending on the solvent used. Comparison of columns 2/3 versus 6/7 in Table 1, and the extensive hydrogen bond network in Figure 7A,B versus Figure 7C,D, show that both chiromers are preferentially solvated by water. However, the unique water cluster identified ($W_1-W_3$) binds significantly more strongly to the W-chiromer than to the M-chiromer (4.32 kcal/mol per rosette, compare column 2 versus 3, Table 1), leading to a preferential stabilization of the W-chiromer in water. Methanol was found to bind more strongly to the W-chiromer, indicating that the latter is also more stable in methanol (1.68 kcal/mol per rosette, compare column 6 versus 7, Table 1). However, as shown in Figure 5F, W-chiromer must overcome an energy barrier in methanol, whereas M-chiromer does not. As a result, the latter forms preferentially in methanol as a kinetic product.

Changes in free energy of binding upon transfer from one solvent to the mixture agree with water being the dominant solvent and W-chiromer being the dominant conformational isomer. In effect, transfer of W-chiromer from water to 50/50 methanol/water, results in a strengthening of free energy of binding of water molecules (10.2 kcal/mol per rosette, compare columns 2 and 4, Table 1). On the other hand, transfer of M-chiromer from methanol to 50/50 methanol/water, results in a weakening of the binding energy of methanol molecules (18.1 kcal/mol per rosette, compare columns 5 and 7, Table 1). This trend suggests a mechanism whereby water molecules play the role of a supramolecular chirality switch involving: (a) water penetration in the RNT grooves and displacement of methanol molecules, (b) establishment of a H-bond network with the exocyclic amino group and pyrimidinic nitrogen, (c) conformational change of the self-assembling module by rotation around the side chain's $CH_2-CH_2-N(\alpha)H_2-C(\alpha)H$ dihedral angle leading to the formation of the thermodynamic W-chiromer. These results demonstrate that methanol acts as a cocatalyst that accelerates RNT self-assembly, whereas contrary to the conventional wisdom in the field, water enhances RNT's relative thermodynamic stability and controls its SC.

**Supramolecular Chirality Is the Result of Conformational Memory.** It is clear from these investigations and earlier reports[1−8] that absolute molecular chirality guarantees some form of SC, but certainly not its profile. The latter is determined by thermodynamic and kinetic parameters defined by the environment in which self-assembly and self-organization took place. Thus, through their hierarchical and conformational states and chiroptical outputs, chiral supramolecular architectures may be viewed as a manifestation of their physical/chemical environment. An important corollary of this statement is that any chiral supramolecular assembly could in principle express multiple chiroptical outputs depending on its physical environment. This, as a result, leads to the conclusion that SC is nothing but an expression of conformational memory.

## Conclusion

We have shown that a *single* chiral molecule can express mirror image chiroptical outputs upon self-assembly into pseudomirror image supramolecular conformational isomers (chiromers). This system is also the first in which mirror-image SC outputs were unambiguously connected to kinetic versus thermodynamic control of a hierarchical self-assembly process. The chiromers were shown to have identical hierarchical organization but expressed mirror-image SC. They were also shown to be thermodynamically stable supramolecular species yet displayed dominant/recessive behavior. Solvent and temperature were shown to play a critical role in determining the dominant chiromer. We have shown that the chiromers memorize and amplify their chirality in an achiral environment, change their chirality in response to the environment (solvent, temperature), and catalytically transfer their SC according to a novel mechanism, thus demonstrating that molecular conformational information can be stored and catalytically propagated.

Extensive experimental and theoretical studies established that the chiromers are solvent-stabilized supramolecular conformational isomers. The solvation models revealed unique arrangements of solvent molecules around the chiromers involved in an extensive network of H-bonds with the exocyclic amino group and/or the pyrimidinic nitrogen of the G∧C base. On the basis of these interactions a mechanism was proposed for SC inversion in which *achiral* solvent molecules (water) play the role of SC switches. These studies have also demonstrated that methanol acts as a cocatalyst that accelerates RNT self-assembly, whereas contrary to the conventional wisdom in the field, water enhances RNT's relative thermodynamic stability and controls its SC.

Finally, while absolute molecular chirality guarantees some form of macromolecular chirality, its profile and amplitude are determined by thermodynamic and kinetic parameters defined by the environment in which self-assembly and self-organization took place. SC may thus be viewed as the result of conformational memory.

## Materials and Methods

All circular dichroism spectra were recorded on a JASCO J-810 spectropolarimeter. Samples were scanned from 350−200 nm at a rate of 100 nm/min. Sample preparations and concentrations are indicated in the figure captions and in the Supporting Information section. Nuclear magnetic resonance experiments were conducted at 5 °C on a Varian Inova-800 spectrometer equipped with either a 5 mm triple axis gradient HCN probe or a 5 mm HCN-Zaxis-gradient cold probe. Atomic force microscopy measurements were performed in tapping mode (TM-AFM) at a scan rate of 2 Hz per line using a Digital Instruments/Veeco Instruments MultiMode Nanoscope IV equipped with an E scanner. Silicon cantilevers (MikroMasch USA, Inc.) with spring constants of 40 N/m were used. TEM imaging was performed on a JEOL 2010 microscope operating at 200 kV. The samples were negatively stained with either 1% uranyl acetate or nano-W (methylamine tungstate, Nanoprobes Inc.). All SEM images were obtained without negative staining, at 5 kV accelerating voltage and a working distance of 3.0 mm on a high-resolution Hitachi S-4800 cold field emission SEM. UV−vis spectra were recorded on an Agilent 8453. Dynamic light scattering (DLS) experiments were performed on a Malvern Zetasizer Nano S working at a 90° scattering angle at 25 °C. This instrument is equipped with a 40 mW He−Ne laser ($\lambda = 633$ nm) and an avalanche photodiode detector. Size distributions were calculated using an inverse Laplace transform algorithm, and the hydrodynamic radii were calculated using the Stokes−Einstein equation.

**Acknowledgment.** We thank NSERC, NRC Canada, and the University of Alberta for supporting this program. We thank the Canadian National High Field NMR Centre (NANUC) for their assistance and use of the facilities. Operation of NANUC is funded by the Canadian Institutes of Health Research, the Natural Science and Engineering Research Council of Canada, and the University of Alberta. The computations were supported

by the Centre of Excellence in Integrated Nanotools at the University of Alberta. We thank Dr. J. G. Moralez for help with AFM imaging.

**Supporting Information Available:** Synthetic procedures for the preparation and characterization of compound **3**; time-dependent CD and VT-CD; 1D and 2D NMR procedures; AFM, TEM and SEM imaging; UV−vis spectroscopy; binary solvent studies; DLS measurements; chiral memory experiments; thermally-induced chirality inversion experiments; catalytic transfer of SC experiments; theory and modeling methods and results; solvation models and associated methods and results. This material is available free of charge via the Internet at http://pubs.acs.org.

JA0706192